MSDM ~~: a~~ v1.0: A machine learning model for precipitation nowcasting over ~~east~~East China using ~~multi-source~~multisource data

Dawei Li, Yudi Liu, Chaohui Chen
Institute of Meteorology and Oceanography, National University of Defense Technology, Changsha 410003, China; davidlilkecookies@126.com (D.L.); chenchaohui2001@nudt.edu.cn (C.C.)

Correspondence to: Yudi Liu (udy.liu@pku.edu.cn)

Abstract. East China is one of the most economically developed and ~~most~~ densely populated areas in the world. Due to its special geographical location and climate, East China is affected by different weather systems ~~like monsoon~~, such as monsoons, shear ~~line, typhoon~~lines, typhoons and extratropical ~~cyclone, in~~cyclones. In the imminent future, the rainfall rate ~~affected by which~~ is difficult to predict precisely ~~predict.~~due to these systems. Traditional physics-based methods ~~like Numerical Weather Prediction~~such as numerical weather prediction (NWP) tend to perform poorly ~~for the~~on nowcasting ~~problem~~problems due to ~~its spinup~~the spin-up issue. ~~Meanwhile~~Moreover, various meteorological stations are distributed ~~here~~in this region, generating a large amount of observation data every day, which has ~~a~~ great potential to be applied to data-driven methods. Thus, it is important to train a data-driven model from scratch that is suitable ~~to~~for the specific weather situation of East China. ~~We collect~~However, due to the high degrees of freedom and nonlinearity of machine learning algorithms, it is difficult to add physical constraints. Therefore, with the intention of using various kinds of data as a proxy for physical constraints, we collected three kinds of data (radar, satellite, and precipitation data) in the flood season from 2017 to 2018 of this area and ~~preprocess~~preprocessed them into ~~ndarray~~tensors (256×256) that cover East China with a domain of 12.8×12.8°. The ~~Multi-Source Data Model (MSDM) which we~~ developed multisource data model (MSDM) combines the ~~Optical~~optical flow, ~~Random~~random forest and ~~Convolutional Neural Network~~convolutional neural network (CNN~~).~~) algorithms. It treats the precipitation nowcasting task as an image-to-image problem, which takes radar and satellite data with ~~a~~an interval of 30 minutes as inputs and predicts radar echo intensity ~~at~~with a lead time of 30 minutes. To reduce the smoothing caused by ~~convolution~~convolutions, we use ~~Optical~~the optical flow algorithm to predict satellite data in the following 120 minutes. The predicted radar ~~echo~~echoes from the MSDM together with satellite data from ~~Optical~~the optical flow algorithm are recursively implemented in the MSDM to achieve a 120~~ minutes~~-minute lead time. The MSDM predictions ~~from MSDM~~ are comparable to those of other baseline models with a high temporal resolution of 6 minutes. To solve ~~the~~ blurry image problems, we applied a modified structural similarity (SSIM) index as a loss function. Furthermore, we use ~~Random~~the random forest algorithm with predicted radar and satellite data to estimate the rainfall rate, and the results outperform those of the traditional~~-~~, nonlinear radar reflectivity factor and rainfall rate (Z-R ~~relationship.~~) relationships that use logarithmic functions. The experiments confirm that machine learning with ~~multi-source~~multisource data provides more reasonable predictions and reveals a better ~~non-linear~~nonlinear relationship between radar echo and precipitation rate. ~~Besides the~~Apart from developing complicated

Style Definition: Comment Text: Font: (Default) Tahoma, 8 pt, English (United States)

Formatted: Font: 12 pt, English (United Kingdom)

Formatted: English (United Kingdom)

Formatted: Normal, Space Before: 9 pt, Don't add space between paragraphs of the same style

Formatted: Normal, Space Before: 6 pt, Don't add space between paragraphs of the same style

Formatted: Normal, Space Before: 6 pt, After: 18 pt

Formatted: Font: Times New Roman

Formatted: Font: Times New Roman

machine learning algorithms~~ will be developed~~, exploiting the potential of ~~multi-source~~multisource data will ~~bring~~yield more improvements.

1. Introduction

In recent years, deep learning and machine learning have achieved great advances with big data. ~~The tremendous~~Tremendous meteorological data are produced every day, which perfectly matches these novel data-driven artificial intelligence (AI) approaches. Quantitative ~~Precipitation Nowcasting~~precipitation nowcasting (QPN) ~~by~~ using ~~Radar Echo Extrapolation~~radar echo extrapolation (REE) ~~have~~has recently become popular ~~recently.~~(Tran and Song, 2019~~a~~). Precipitation ~~Nowcasting makes the prediction of~~ nowcasting predicts rainfall intensity in the following ~~several~~few hours. Based on various data with high ~~spatio-temporal~~spatiotemporal resolutions, ~~the~~ AI precipitation prediction can be relatively accurate compared with traditional numerical weather prediction (NWP) methods. U-Net (Ronneberger et al., 2015) is a well-known network designed for image segmentation, and its core is upsampling, downsampling, and skip connection. It can efficiently achieve high accuracy with a small number of samples. Agrawal et al.(~~Agrawal et al.,~~ 2019) treated ~~the~~ precipitation nowcasting as an image-to-image problem. They employed ~~the~~ U-Net (Ronneberger et al., 2015) to predict the change ~~of~~in radar echo for QPN, which is superior to ~~NOAA's~~ High Resolution Rapid Refresh (HRRR) numerical prediction from the National Oceanic and Atmospheric Administration (NOAA) when the prediction time is within 6 hours. Sonderby et al.~~(Sønderby et al., n.d.)~~(2020)~~ proposed a MetNet to discover the weather pattern from radar and satellite data which can predict the next 8 hours precipitation with a resolution of 1 kilometer in 2-minute intervals. Shi et al.(Shi et al., n.d.) used the Convolutional Long Short-Term Memory (ConvLSTM) to predict the spatiotemporal sequences of the precipitation. And they also provide the first benchmark as well as a new TrajGRU model to capture the spatiotemporal correlations(Shi et al., n.d.). Also, in the field of video prediction, Wang et al. proposed various recurrent networks like PredRNN++ (Wang et al., 2018), MIM(Wang et al., 2019b), E3D-LSTM(Wang et al., 2019a). However, their work is based on a slight modification of existing techniques demanding massive computing resource to train and haven't been applied to the numerous meteorological data.~~ proposed a neural weather model (NWM) called MetNet that uses axis self-attention (Ho et al., 2019) to discover weather patterns from radar and satellite data. MetNet can predict the next 8 hours of precipitation in 2-minute intervals with a resolution of 1 kilometer. Shi et al. (2015) treated precipitation nowcasting as a problem of predicting spatiotemporal sequences and modified the fully connected long short-term memory (FC-LSTM) by replacing the Hadamard product with a convolution operation in the input-to-state and state-to-state transitions. They believe that cloud movement is highly uniform in some areas, and convolutions can capture these local characteristics. Therefore, the convolution operation in the input transformations and recurrent transformations of their proposed convolutional LSTM (ConvLSTM) helps to handle the spatial correlations. Furthermore, they apply the same modification to the gated recurrent unit (GRU) and notice that convolution is location-invariant and focuses on only a fixed location because its hyperparameters (kernel size, padding, dilation) are fixed. However, in the QPN problem, a specific location of cloud clusters continuously changes over time. Hence, Shi et al. (2017) proposed a trajectory GRU (TrajGRU) that uses a subnetwork to output a location-variant connection structure before state transitions. The dynamically changed connections help TrajGRU capture the trajectory of cloud clusters more accurately than previous methods. In the field of video prediction, Wang et al. proposed various recurrent neural networks (RNNs) based on LSTM. For example, they designed PredRNN++ (Wang et al., 2018) with a cascaded dual memory structure and gradient highway unit, which strengthens the power for modeling short-term dynamics and alleviates the vanishing gradient problem, respectively. In addition, to capture spatial characteristics through recurrent state transitions, Wang et al. (2019a) integrated 3D convolutions inside LSTM units and proposed Eidetic 3D LSTM (E3D-LSTM). Moreover, Wang et al. (2019b) designed the memory in memory (MIM) network to handle higher-order nonstationarity of spatiotemporal data. By using differential signals, MIM can model the nonstationary properties between adjacent recurrent states. However, their work is based on a slight modification of existing techniques demanding massive computing resources for model training and has not been applied to big meteorological data.

Computer vision techniques have long been used in object detection, video prediction, and human motion prediction~~, etc~~. Tran and Song ~~(Tran and Song, 2019b)~~(2019) used image quality assessment techniques as a new loss function instead of the common mean squared error (MSE), which ~~will mislead~~misled the process of training and ~~generate the~~generated blurry ~~image. Optical flow methods simply describe the position and velocity of the radar echo with a constant velocity.~~images. Ayzel et al. (~~Ayzel et al.,~~ 2019) designed an advanced model based on the multiple optical flow algorithm for QPN, but it still performs ~~badly~~poorly in the prediction of the onset and decay of precipitation systems~~.~~ ~~Hence, to make full use~~ because optical flow methods simply calculate the position and velocity of the radar echo with a constant velocity rather than consider the changing intensity of radar echo.

On the one hand, the current massive ~~meteorological~~ amounts of data ~~combining Optical Flow methods and Deep~~are underutilized; on the other hand, scientists in the field of machine learning ~~are conducted to predict the QPN~~focus on pursuing high accuracy by increasing the complexity of models based on ~~the characteristics of multi-~~a single source of data~~, such as radar echo, Infrared~~. Given this background, from the perspective of atmospheric science, we build a multisource data model (MSDM) with the aim of fully using multisource observation data (for example, radar reflectivity, infrared satellite data, and ~~observation data et al.,~~rain gauge data) and find suitable machine learning algorithms (for example, deep neural network, optical flow, and random forest algorithms) for each type of data that can ensure accuracy while saving computing resources. In addition, due to the high degrees of freedom and nonlinearity of neural networks, it is difficult to apply physical constraints to these machine learning models. Hence, we hope that multisource data will function as a proxy for physical constraints to guide the model during the training process. The main advantage of MSDM lies in its transferability: any machine learning model and observation data can be incorporated into the model. For example, wind speed data can be a proxy for dynamic constraints, and temperature data can function as a proxy for thermodynamic constraints. Due to the limit of computing resources, the aim of this paper is not to achieve a higher resolution or ~~accuracy of the~~ prediction accuracy but to propose a method ~~of~~ combining ~~Optical Flow~~machine learning and ~~CNN~~deep learning with radar echo data, satellite data, and automatic ground observation data to ~~make~~achieve physically reasonable QPN.

The dataset and methods used ~~for~~in this study are described in section 2. Section 3 shows the results. Section 4 draws conclusions and discusses some possible future work.

2. Materials and Methods

2.1 Dataset

The spatial and temporal distribution characteristics of precipitation are related to many factors ~~like~~, such as the terrain, atmospheric circulation, and climatic conditions~~, etc~~. To train ~~the Deep~~a deep learning model ~~to learn~~that can capture the precipitation characteristics of East China, we collected ~~multi-source~~multisource observation data of the flood season (May to September) for a total of 306 days from 2017 to 2018. Due to the missing radar data from May 1 to 9 and September 26 to 30, 2018, ~~the radar data is~~ there are only 292 days of radar data in total. The missing data are obtained by interpolating the data ~~at the~~from adjacent moments. Among the data, ~~Precipitation~~the precipitation data of regional automatic ground stations in East China with a time interval of 10 minutes are shown in Fig 1.

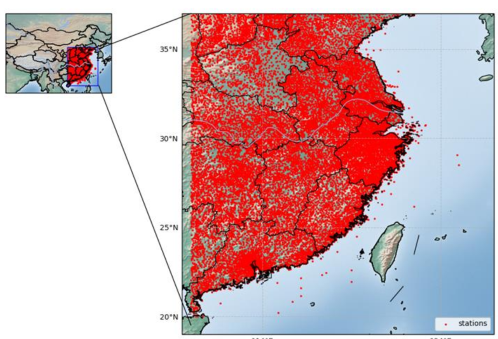

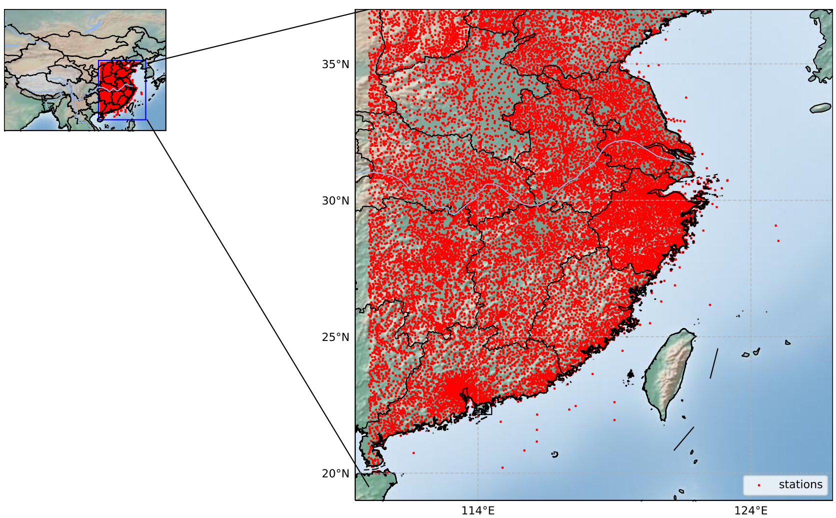

Figure 1. Distribution of the automatic ground stations in East China.

The weather radar data (resolution of 0.5°×0.5°) have been preprocessed into the combined reflectivity~~, whose~~; the latitude range is from 21.0°N to 36.0°N, the longitude range is from 112.0°E to 125.9°E, and ~~was~~data were available every 6 minutes (Fig 2(a)). The Himawari 8 satellite brightness temperature data (resolution 0.5° × 0.5°) for ~~channel~~channels 07-16 are used with a latitude range of 19-37°N, a longitude range of 110-127~~-~~°E, and a time interval of 30 minutes (Fig 2~~-~~(b)). The links for the datasets are as follows:

Radar data: http://data.cma.cn/data/detail/dataCode/J.0012.0003.html,

AWS data: http://data.cma.cn/data/detail/dataCode/A.0012.0001.html,

Himawari 8 satellite data: http://www.cr.chiba-u.jp/databases/GEO/H8_9/FD/index.html.

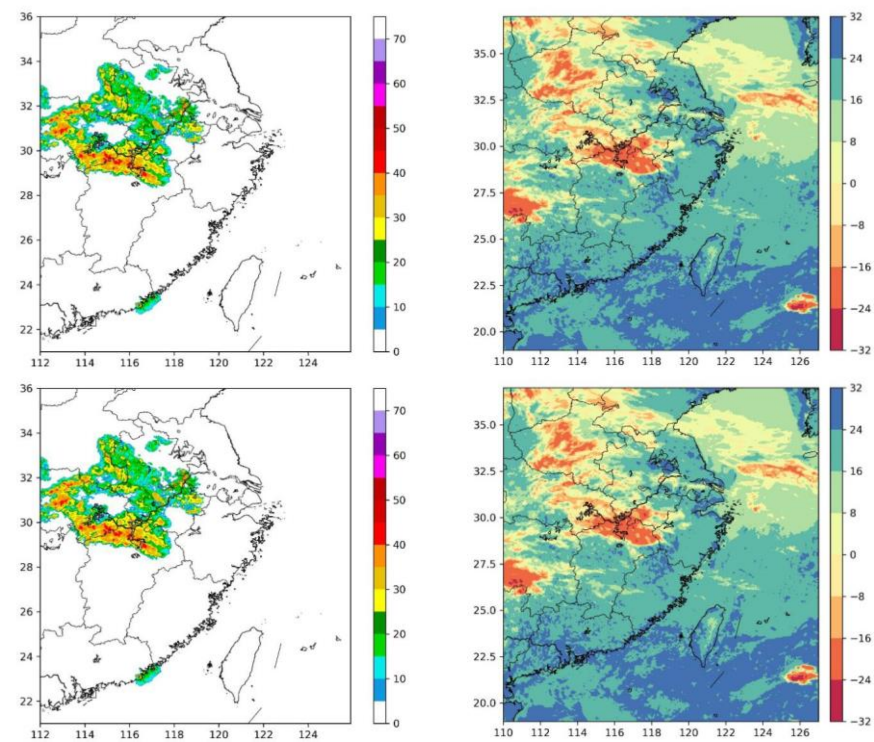

(a) (b)

Figure 2. Combined reflectivity (~~Unit~~unit: dBZ) in East China (a), Himawari 8 satellite brightness temperature data (~~Unit~~unit: ℃) of channel ~~7~~07 (b) on May 1, 2017.

~~2.2 Methods~~

~~To test our method, we compared with the optical flow method, ConvLSTM, U-net methods. Due to the limit of the computational resource, we use the sequence of 5 frames before time t to predict the following 5 frames. Then, the output results are used to further predict the radar echo (Fig 3).~~

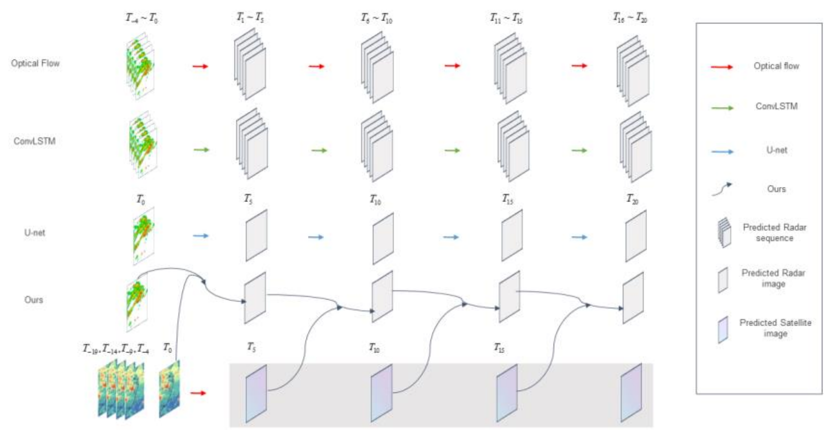

~~Figure 3. The time sequences of the optical flow, ConvLSTM, U-net and our method~~

Model Description

Model Architecture

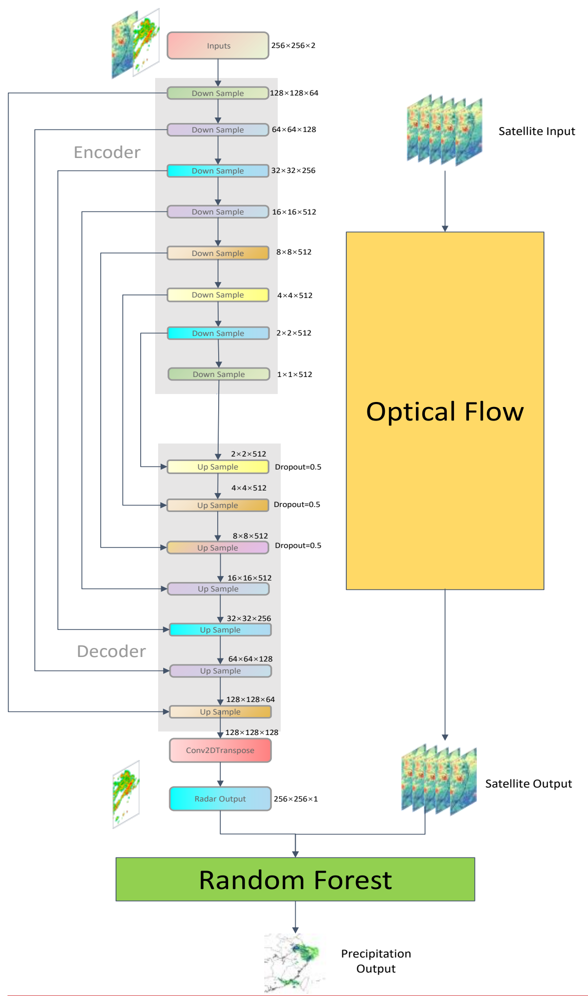

Figure 3. Structure of the MSDM.

To incorporate multisource data, we designed an MSDM with three parts: deep learning, optical flow, and random forest (Fig 3). The deep learning part of the MSDM is inspired by the state-of-the-art U-Net (Ronneberger et al., 2015) designed for image segmentation. It follows the encoder-decoder structure that encoder has 8 down sample blocks and decoder has 7 up sample blocks. Each downsampling block in the encoder consists of Conv2D, batch normalization, and leaky rectified linear unit (LeakyReLU) activation layers. Each upsampling block in the decoder includes transposed convolutional, batch normalization, dropout of 0.5 (applied to the first 3 blocks), and ReLU activation layers. In each convolutional layer, the step size parameter (stride) is set to 2, and padding is set to 'same'. The kernel size varies between 4×4 and 2×2 to extract the spatial characteristics at different scales. The batch normalization layer effectively avoids the gradient disappearance problem and improves the convergence speed. We use dropout to randomly discard some information with a probability of 50% to prevent overfitting. The activation function adds nonlinearity to each block and allows the model to better learn the nonlinear relationship between the input and target. Transposed convolutional layers are introduced to substitute upsampling layers in U-Net to increase the resolution of the images. As in U-Net, there are skip connections between the encoder and decoder to solve the problem of gradient explosion and gradient disappearance during training.

The primary reason that we use transposed convolutional layers to replace upsampling layers is that both layers are used for upsampling images. Upsampling layers use an interpolation method (for example, nearest neighbor interpolation, bilinear interpolation, and bicubic interpolation) to rescale the input image to a desired size with a higher resolution. These interpolation methods are preset, so there is little room for the network to learn. The deconvolution operation is not a predefined interpolation method, and it has some learnable parameters to convert the output to the original image resolution. Through the training of the model, it will learn an optimal upsampling method instead of a preset method.

In the deep learning part, the MSDM takes the array with a shape of 256×256×2, which represents the height, width and channel of the image. Radar and satellite grid point data are at different channels. The output of this part is a predicted radar image 30 minutes later with a shape of 256×256×1. The optical flow part takes 5 consecutive satellite frames as input to extrapolate the satellite image in the following 2 hours. Subsequently, the predicted radar image and satellite image will be used in two parts. First, it will flow into the random forest part to estimate the precipitation rate. Second, it will be recursively used as the input of the deep learning part to achieve a lead time of two hours.

The reasons why we do not predict precipitation directly using deep learning are as follows: 1) The precipitation data we collected are irregular site data, which are distributed only on land and do not include precipitation on the sea (Fig 1). The combined radar reflectivity (Fig 2(a)) and Himawari 8 satellite data (Fig 2(b)) are regular grid point data and include sea data. The spatial distributions of these three types of data are inconsistent, so it is impossible to make a feature-label correspondence to directly predict precipitation. 2) The use of shapefiles to extract radar echo or satellite data on land will cause the edge of the echo to be limited to the land, which loses the meaning of extrapolation. 3) We hope to improve the transferability of MSDM that can integrate different kinds of data except grid point data. Therefore, the method of processing precipitation data can be used on other observation site data in daily operation. 4) We believe that deep learning efficiently extracts the long-period trend in precipitation, but it cannot capture the transient characteristics of precipitation. Therefore, for each rainfall event, we use random forest to model the nonlinear relationship between multisource data to capture its unique characteristics.

Reference Models

2.2.1 Optical flow method

We first employed ~~the~~ rainy motion v1, an optical flow model proposed by Ayzel et al (~~Ayzel et al.,~~ 2019), to ~~see~~evaluate the performance of the optical flow algorithm for tracking and extrapolating radar ~~echo~~echoes by our dataset. It performs poorly on the radar echo data when the ~~leading~~lead time is up to 60 minutes. However, it performs better on satellite data, which ~~is~~are recorded every 30 minutes. We believe that ~~the~~ cloud layer motion is dominated by air advection transportation~~,~~; thus, the optical flow method can better simulate its motion characteristics. ~~Also, the larger intervals between two~~Additionally, the temporal resolution of satellite data is coarser (30 minutes), so we can directly obtain the sequence of four frames ~~make it~~ of the following 2 hours through one prediction rather than iterative prediction. Optical flow can predict ~~better because it extrapolates fewer frames for~~such short sequences quickly and shows great advantages in saving computing resources and avoiding error accumulation. In addition, the ~~satellite data than those for the radar echo data at the same lead time. Convolution~~main drawback of the convolution operation is that it smooths the characteristics of the image, and the level of smoothness increases when applying convolutions recursively in deep learning models ~~not only learn the decay and initiation of radar echo, but also smooth the characteristics, which would increase its level through recursive application.~~. Therefore, to ease the smoothing of radar ~~echo~~echoes and preserve more details of precipitation systems, we decide to use the results of ~~predicted~~ satellite data predicted by the optical flow ~~in~~component of our ~~multi-input models to save characteristics of precipitating system~~model.

2.2.2 ConvLSTM

ConvLSTM (Shi et al., ~~n.d.)~~2015) ~~was one of the most classic models~~is a traditional model for the ~~precipitation nowcasting~~QPN problem. Hence, we compare our model with ConvLSTM to see whether the model with ~~multi-source~~multisource data performs well when we simply formulate ~~precipitation nowcasting~~QPN as an image-to-image problem rather than ~~spatio-temporal~~ a spatiotemporal sequence problem (Eq. 1).

$$\tilde{\mathcal{X}}_{t+1},\ldots,\tilde{\mathcal{X}}_{t+5} = \underset{\mathcal{X}_{t+1},\ldots,\mathcal{X}_{t+5}}{argmax}\; p(\mathcal{X}_{t+1},\ldots,\mathcal{X}_{t+5} \mid \mathcal{X}_{t-5+1},\mathcal{X}_{t-5+2},\ldots,\mathcal{X}_t), \qquad (1)$$

Tensor $\mathcal{X}_t$ represents the radar echo map in the shape of 256×256 at time t, and tensor $\tilde{\mathcal{X}}_{t+1}$ represents the model prediction result.

Formatted: Font: Bold
Formatted: Normal, Level 3, Space Before: 12 pt, After: 12 pt, Keep with next
Formatted: Font: Bold
Formatted: Normal, Level 3, Space Before: 12 pt, After: 12 pt, Keep with next
Formatted: Font: Font color: Black, (Intl) Palatino Linotype
Formatted: Font: Font color: Black, (Intl) Palatino Linotype
Formatted: Font: Font color: Black, (Intl) Palatino Linotype
Formatted: Normal, Don't adjust right indent when grid is defined, Line spacing: At least 13 pt, Don't snap to grid
Formatted: Font: Font color: Black, (Intl) Palatino Linotype
Formatted: Font: Font color: Black, (Intl) Palatino Linotype
Formatted: Font: Font color: Black, (Intl) Palatino Linotype
Formatted: Font: Font color: Black, (Intl) Palatino Linotype
Formatted: Font: Font color: Black, (Intl) Palatino Linotype
Formatted: Font: Font color: Black, (Intl) Palatino Linotype
Formatted: Font: Font color: Black, (Intl) Palatino Linotype
Formatted: Font: Font color: Black, (Intl) Palatino Linotype
Formatted: Font: Font color: Black, (Intl) Palatino Linotype
Formatted: Font: Font color: Black, (Intl) Palatino Linotype
Formatted: Font: Font color: Black, (Intl) Palatino Linotype
Formatted: Font: Font color: Black, (Intl) Palatino Linotype
Formatted: Font: Font color: Black, (Intl) Palatino Linotype
Formatted: Font: Font color: Black, (Intl) Palatino Linotype
Formatted: Font: Font color: Black, (Intl) Palatino Linotype
Formatted: Font color: Black
Formatted: Font: Font color: Black, (Intl) Palatino Linotype
Formatted: Font: Font color: Black, (Intl) Palatino Linotype
Formatted: Font: Font color: Black, (Intl) Palatino Linotype
Formatted: Font: Font color: Black, (Intl) Palatino Linotype
Formatted: Font: Font color: Black, (Intl) Palatino Linotype
Formatted: Font: Font color: Black, (Intl) Palatino Linotype
Formatted: Font: Font color: Black, (Intl) Palatino Linotype
Formatted: Font: Font color: Black, (Intl) Palatino Linotype
Formatted: Font color: Black
Formatted: Font: Palatino Linotype, Font color: Black

2.2.3 ~~Multi-~~U-Net

U-Net (Ronneberger et al., 2015) was employed by Agrawal et al. (2019) for QPN. They treat the problem as an image-to-image problem (Eq. 2) to forecast the precipitation in the next hour.

$$\widetilde{\mathcal{X}}_{t+5} = \underset{\mathcal{X}_{t+5}}{argmax}\, p(\mathcal{X}_{t+5} \mid \mathcal{X}_t), \quad (2)$$

Tensor $\mathcal{X}_t$ and $\widetilde{\mathcal{X}}_t$ is as in Eq. 1, we use the U-Net architecture to predict the radar image 30 minutes later in comparison to the MSDM to demonstrate that the combination of multisource data is better than single source ~~Data~~ data.~~Model (MSDM)~~

Training and evaluation method of the MSDM

The model ~~which~~that we designed is a modified U-~~net~~Net model (Fig ~~4). Each downsample block in the encoder consists of Conv2D, Batchnorm, Leaky ReLU. Each upsample block in the decoder is Transposed Conv, Batchnorm, Dropout of 0.5 (applied to the first block), ReLU. As in U-net, there are skip connections between the encoder and decoder.~~3). We use the radar and satellite data as inputs, and the output is the intensity of the radar echo after half~~-~~ an hour (Eq. ~~2~~3). The two kinds of data were fed into the encoder~~,~~ and then ~~they were~~ concatenated by skip connections and ~~flow~~flowed into the decoder and transposed ~~convolution~~convolutional layer (Fig ~~4~~3).

$$\widetilde{\mathcal{X}}_{t+5} = \cancel{\underset{\mathcal{X}_{t+5}}{argmax}}\underset{\mathcal{X}_{t+5}}{argmax}\, p(\mathcal{X}_{t+5} \mid \mathcal{X}_t, \mathcal{Y}_t), \quad \cancel{(2)}\ (3)$$

~~Our model wants to use the~~The MSDM uses weather radar echo data $\mathcal{X}_t$ and Himawari 8 satellite brightness temperature data $\mathcal{Y}_t$ to predict the radar echo map at time t+5. ~~Then~~After the first round of prediction, we combined $\widetilde{\mathcal{X}}_{t+5}$ from our model and the predictions of $\widetilde{\mathcal{Y}}_{t+5}$ from ~~Optical~~optical flow for further prediction. During preprocessing, the weather radar data and Himawari 8 satellite brightness temperature data are extracted, which cover the area of 23.0-35.8°N, 113.0-125.8~~-~~°E with a 256×256 window. Then, the ~~value~~values of these data Z are transformed into pixels P by Eq. ~~3~~ 4

$$P = \frac{Z - min\{Z\}}{max\{Z\} - min\{Z\}}, \quad (\cancel{3}\ 4)$$

~~In order to~~To improve the image quality~~ of images~~, we apply a modified structural similarity index (SSIM~~)~~) (Wang et al., 2004) as the loss function, which is helpful to solve ~~the~~ blurry image problems. The loss function for the predicted image and ground truth is defined ~~as~~by Eq. ~~4~~5:

$$Loss = -1 \times SSIM(y_{pred}, y_{true}) = -1 \times \frac{(2\mu_{y_{pred}}\mu_{y_{true}} + C_1)(2\sigma_{y_{pred}y_{true}} + C_2)}{(\mu^2_{y_{pred}} + \mu^2_{y_{true}} + C_1)(\sigma^2_{y_{pred}} + \sigma^2_{y_{true}} + C_2)}, \quad (\cancel{4}\ 5)$$

~~In which~~where y_{pred} is the predicted image, y_{true} is the ground truth, and $\mu_{y_{pred}}$ and $\mu_{y_{true}}$ are the average ~~value~~values of y_{pred} and y_{true}, respectively. $\sigma^2_{y_{pred}}$ and $\sigma^2_{y_{true}}$ are ~~variance~~the variances of y_{pred} and y_{true}, respectively. $\sigma_{y_{pred}y_{true}}$ is the cross-correlation of y_{pred} and y_{true}. $C_1$and C_2 are small positive constants. In each calculation, a window of 3×3 is taken from

Formatted: Font: Bold

Formatted: Normal

Formatted: Font: Times New Roman

the image, and then the window is continuously sliding for calculation~~, and finally~~. Finally, the average value is taken as the global SSIM.

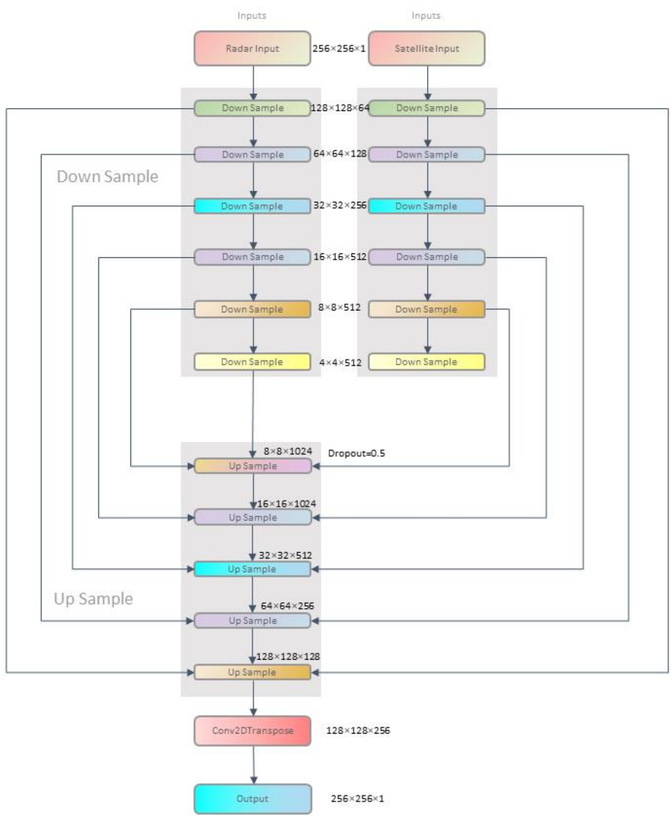

~~**Figure 4. Structure of Multi-source Data Model**~~

~~3. Results~~

~~3.1. REE~~

To ~~test if~~evaluate our model, a comparison was made between the ~~multi-source data can help to improve REE~~optical flow method, ConvLSTM, and ~~QPN tasks.~~ U-Net methods. Due to limits on computational resources, we use a few frames to predict the results for the half-hour. Then, the output results are used to iteratively predict the radar echo in the next half-hour to achieve a lead time of 2 hours (Fig 4). For the baseline sequence-to-sequence models (ConvLSTM, optical flow), we use the first 5 frames (T_{-4}~T_0) to predict a sequence of the next 5 frames (T_1~T_5) and use this result to iteratively predict the remaining three sequences (T_6~T_{10}, T_{11}~T_{15}, T_{16}~T_{20}). For image-to-image models (U-Net, MSDM), we use frame T_0 to predict frame T_5 and use this prediction as input to iteratively predict the following frames (T_{10}, T_{15}, T_{20}).

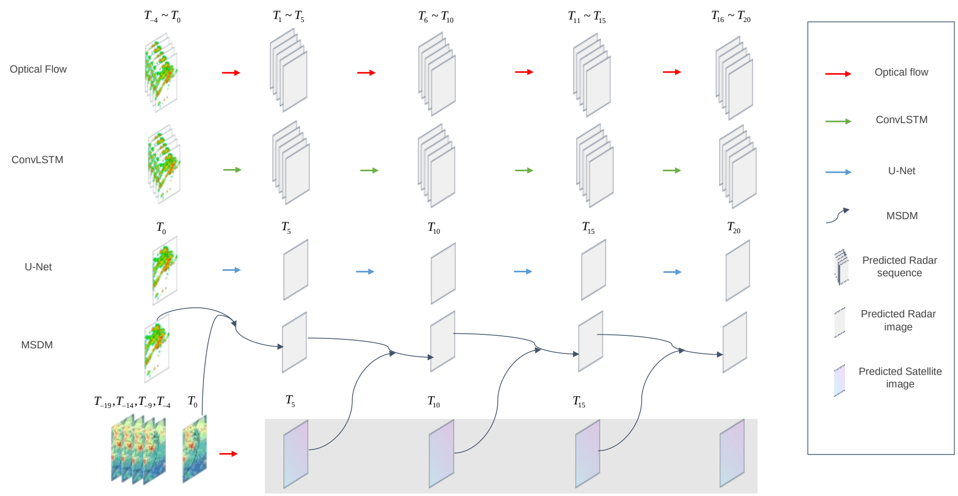

Figure 4. The time sequences of the optical flow, ConvLSTM, U-Net and MSDM.

Performance Evaluation

The MSDM is trained with our dataset on Google Colab ~~pro~~Pro with ~~Tensorflow~~TensorFlow-GPU-2.2.0 and executed on an NVIDIA Tesla P100 GPU (~~16GB).~~16 GB). In total, 240 days of data ~~are~~ used for training, 26 days for ~~validating~~validation and 26 days for testing. All the models are compiled with the Adam optimizer, and the learning rate is set at 0.001. To avoid overfitting, we apply the early-stopping strategy to monitor the loss ~~of validation set. The critical success index (CSI=~~$\frac{hits}{hits+misses+falsealarms}$~~) is used to show the performance of different models. Other similar scores do the same work, so we~~

~~do not take them~~in the validation set. We use several metrics to evaluate the model's performance on the test set, namely, the critical success index (CSI, Eq. 6), Heide skill score (HSS, Eq. 7), false alarm ratio (FAR, Eq. 8) (Woo and Wong, 2017), root mean square errors (RMSEs), and use the SSIM to evaluate the structural similarity between the generated image and target image.

$$\mathrm{CSI}=\frac{\text{hits}}{\text{hits}+\text{misses}+\text{false alarms}}, \tag{6}$$

$$\mathrm{HSS}=\frac{2(\text{hit}\cdot\text{correct negative}-\text{miss}\cdot\text{false alarm})}{\text{miss}^2+\text{false alarm}^2+2\cdot\text{hit}\cdot\text{correct negative}+(\text{miss}+\text{false alarm})(\text{hit}+\text{correct negative})}, \tag{7}$$

$$\mathrm{FAR}=\frac{\text{false alarm}}{\text{hit}+\text{false alarm}}, \tag{8}$$

where the correct negatives, hits, misses and false alarms are determined by the threshold value. Woo and Wong (2017) provide more details about these metrics. We applied six thresholds of 0.1, 1, 5, 10, 25, and 40 dBZ to calculate the CSI, HSS and FAR. To stress the importance of areas with large radar reflectivity, we assign a weight $w(\text{threshold})$ (Eq. 9) to different thresholds and calculate the weighted CSI and HSS (the larger the better).

$$w(\text{threshold})=\begin{cases}1, & \text{threshold}=0.1\\ 1, & \text{threshold}=1\\ 2, & \text{threshold}=5\\ 3, & \text{threshold}=10\\ 5, & \text{threshold}=25\\ 8, & \text{threshold}=40\end{cases}, \tag{9}$$

We set all the weights to 1 for the FAR (the smaller the better) because we believe that the influence of false alarms of every threshold is the same. The RMSE is used to evaluate the global error of the predicted radar image. For the SSIM, we set the Gaussian filter size to 3×3 and the width to 1.5 to evaluate the local structural similarity between the generated image and target image.

3. Results

3.1 REE

In the region we select over ~~east~~East China, the radar echo ~~as well as~~and precipitating cloud ~~changes~~system change little between two adjacent frames (6 minutes). Therefore, the results of all the models are shown every 30 minutes (Fig 5). The input of ~~Optical~~optical flow and ConvLSTM is a sequence of 5 frames before time 0, and the output is a sequence of 5 frames in the following half-hour. The input of U-~~net~~Net is a single frame of the radar echo data at time 0, and the input of the MSDM includes a frame of satellite data and a frame of the radar echo data. When the output of the first 30 minutes is ~~got~~obtained, we take it as the input to replace the real data for further prediction. After the first step of prediction, the satellite data are input into the MSDM ~~to predict~~for QPN by the ~~Optical~~optical flow algorithm. Because ~~the movement of the~~ cloud ~~was~~ movements are dominated by ~~the~~ advective motion, the ~~Optical~~optical flow method is used.

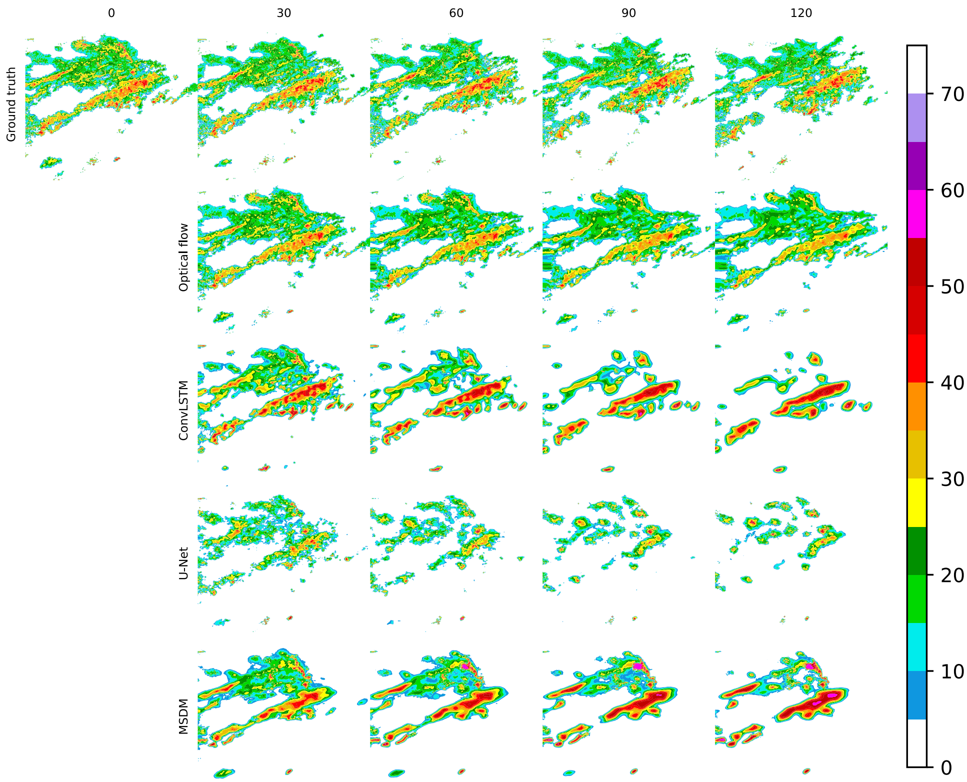
0
30
60
90
120
Ground truth
Optical flow
ConvLSTM
U-Net
MSDM
70
60
50
40
30
20
10
0

(a)

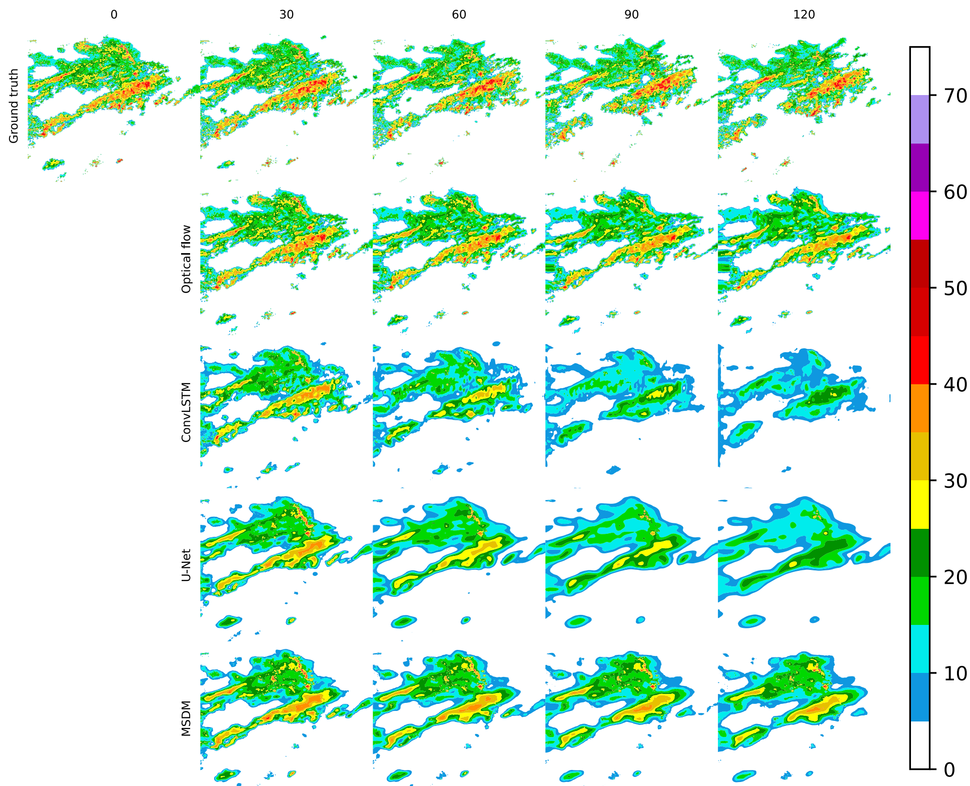

(b)

Formatted: Font: Bold

Formatted: Normal

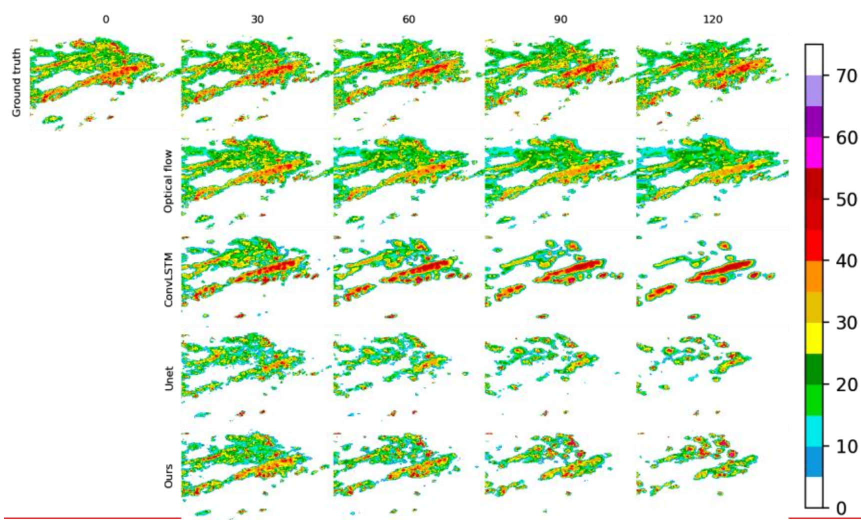

Figure 5. Illustrations of the observed radar echo, the radar echo simulated ~~one~~ by the optical flow, ConvLSTM, U-~~net~~Net and MSDM. For the ~~Optical~~optical flow and ConvLSTM, we select one frame every half-hour for comparison with other models. In Fig 5(a), each model was trained with the modified SSIM. In Fig 5(b) each model was trained with the MSE. The date and time are September 7, 2018, 00:00.

~~In Fig 5, the~~In Fig 5, we present the comparison of 4 models trained with different loss functions. Fig 5(a) shows that the models trained with the modified SSIM predict many large-value areas of radar echo because the SSIM can extract the local structural similarity through the training process. In contrast, Fig 5(b) shows that models trained with the MSE tend to smooth the details of radar echo and seldom predict large radar echo values because the large-value area is only a small part of the entire echo, and the MSE will ignore these areas when it optimizes errors on a global scale. Hence, the modified SSIM shows its advantage when compared with the conventional loss function in the REE task.

The radar echoes predicted by the ConvLSTM, U-~~net~~Net and MSDM decay in the following 2 hours, while ~~the radar echoes~~those predicted by the ~~Optical~~optical flow method ~~always keep.~~remain stable. Thus, the ~~Optical~~optical flow method ~~could~~can perfectly predict the edge and shape of the radar echo, which is the reason why it ~~gets~~obtains the highest average weighted CSI ~~score with the threshold~~at a lead time of ~~0.1dBZ~~30 minutes (Table 1) on the testing set. However, the fatal weakness of the ~~Optical~~optical flow method is that ~~the predicted radar echo intensity is larger than the observed one~~it simply predicts radar echo movement from previous images without predicting radar echo decay and initiation, which ~~leads to the lowest CSI score with the threshold of 40 dBZ~~ causes its accuracy to decrease over time (Table ~~2). Besides, it cannot extrapolate the tail of radar echo because it tracks features by the~~ 1), and the FAR keeps increasing (Table 3). In addition, it employs an algorithm called a corner detector~~(Ayzel et al., 2019). We notice that the~~ (Ayzel et al., 2019) to identify special points from previous frames and track the movement of these points. When it extrapolates the tail of the radar echo, it cannot find corresponding points from previous images because the tail of the radar echo at this moment was in a position outside the radar image of previous frames. Consequently, unreasonable shapes exist in the tail of the predicted radar echo. In Fig 5(a), we find that ConvLSTM performs the best for the strong echoes, but it cannot maintain the shape of the echo. ~~Also~~Additionally, there exists a phenomenon ~~that~~in which only the strong~~-~~ echo area is increasing~~ solely~~, while the weak~~-~~ echo area is continuously decreasing, which is contradictory according to ~~the~~ fluid continuity theory. The ConvLSTM captures the temporal features from previous frames, which strengthens the intensity, but it ~~could not~~cannot properly predict the initiation and decay of the whole system. ~~That~~This finding could explain why it ~~gets the highest CSI scores with a threshold of 40 dBZ, but it looks quite different from ground truth after 60 minutes.~~ obtains the lowest FAR in the last hour (Table 3) because the fewer the number of predicted echoes, the lower the ratio of making mistakes is.

~~The~~ ConvLSTM is prone to error accumulation due to ~~the~~ iterative training and ~~needs~~requires massive computing resources~~.~~ ~~So we decide to~~ (Yu et al., 2018). Therefore, we use a convolutional neural network (CNN) as a substitute to treat REE as an image-to-image problem. U-~~net~~Net along with our MSDM ~~could~~can generally simulate the motion of the radar echo ~~with~~while maintaining its outline, but the MSDM with ~~the~~ satellite data ~~could~~can avoid ~~the~~ radar echo ~~decaying~~decay through iterations. ~~Our~~The MSDM ~~ranks second with a threshold of 40dBZ (Table 2) and performs relatively well in the first hour~~ has comparable performance with ~~a threshold of 0.1dBZ (Table 1).~~baseline models and outperforms other models in the short-term period (Table 1 and Table 2). We believe it ~~keeps~~retains the merits of the ~~Optical~~optical flow method, which can maintain the ~~pattern~~shape of the radar echo, ~~as well as~~and it has the ability to ~~predicting~~predict the strong~~-~~ echo area from U-~~net. When~~ Net. The MSDM performs poorly when the lead time is longer than ~~60~~90 minutes~~, the MSDM performs poorly,~~ because the ~~accumulative~~cumulative error from the two kinds of data was larger than either of both. ~~Besides, the~~In addition, satellite data may provide more details that the radar echo may not contain, for example, data over the sea~~,~~; instead, these details may be treated as noise or false ~~alarm~~alarms, so the ~~CSI scores~~accuracy will ~~be lower~~decrease.

~~**Table 1.** CSI of four models with the threshold of~~ Table 1 and Table 2 show the weighted average CSI and HSS on the test set with different thresholds (0.1, 1, 5, 10, 25, 40, unit: dBZ). The two metrics are used to evaluate the performance of each model (the higher the better). From Table 1, we notice that optical flow method achieves the best score when the lead time is 30 minutes, which shows its great advantage in short-term forecasting. However, its long-term predictions are not accurate due to a lack of simulation of the radar echo evolution. ConvLSTM performs poorly because it increases only the strong echo but neglects the prediction of low-value areas. Hence, even though it obtains high scores on large reflectivity areas, its weighted CSI and HSS are still lower than those of the other models. U-Net also performs poorly due to its inability to handle temporal correlations and the absence of key spatial information. The MSDMs with different loss functions (MSE and SSIM) perform well in long-term forecasting. The SSIM can capture the structural similarities of radar images, while the MSE can calculate the global errors. However, SSIM is prone to error accumulation through iterative prediction. Therefore, in Table 1, MSDM_ssim ranks best for lead times of 60 minutes and 90 minutes, while MSDM_mse ranks best for other lead times. Satellite data add more spatial information for the MSDM to learn and set physical constraints on it. Therefore, the MSDM best scores in the first three moments of the weighted HSS. Regarding the FAR, the MSDM still performs best in the first two moments due to its reasonable prediction of the shape and intensity of the radar echoes. ConvLSTM ranks best in the last two moments because it forecasts only strong echoes of a few areas, which greatly reduces the probability of false alarms.

Table 1. Weighted average CSI on the test set with different thresholds (0.~~1dBZ at the 30th min, 60th min, 90th min and 120th min.~~1, 1, 5, 10, 25, 40, unit: dBZ). The best ~~score is~~scores are highlighted in bold~~ face~~. The second-best score is underscored (the larger the better).

Model	30 min	60 min	90 min	120 min
Optical Flow	**0.~~6917~~414**	0.~~6004~~303	0.~~**5433**~~209	0.~~5037~~205
~~MSDM~~ConvLSTM	0.~~6344~~399	0.~~**6065**~~269	0.~~4663~~211	0.~~3813~~157
~~ConvLSTM~~U-Net	0.~~5688~~348	0.~~5532~~259	0.~~5384~~216	0.~~**5143**~~184
~~U-net~~MSDM_mse	0.~~6282~~362	0.~~5661~~286	0.~~5014~~245	**0.~~4484~~218**
MSDM_ssim	0.405	**0.317**	**0.258**	0.217

~~**Table 2.** As in Table 1 except the threshold of 40dBZ~~

Table 2. Weighted average HSS on the test set with different thresholds (0.1, 1, 5, 10, 25, 40, unit: dBZ). The best scores are highlighted in bold. The second-best score is underscored (the larger the better).

Model	30 min	60 min	90 min	120 min
Optical Flow	0.~~1589~~512	0.~~0894~~409	0.~~0586~~34	**0.~~0411~~304**
~~MSDM~~ConvLSTM	0.~~1836~~487	0.~~1559~~311	0.~~1280~~246	0.~~1147~~18
U-Net	0423	0.307	0.25	0.209
~~ConvLSTM~~MSDM_mse	0.~~**2711**~~437	0.~~**1739**~~341	0.~~1203~~29	0.~~0857~~255
~~U-net~~MSDM_ssim	**0.~~1816~~514**	**0.~~1557~~413**	**0.~~1368~~343**	0.~~**1215**~~291

Table 3. Average FAR on the test set with different thresholds (0.1, 1, 5, 10, 25, 40, unit: dBZ). The best scores are highlighted in bold. The second-best score is underscored (the smaller the better).

Model **90 min**

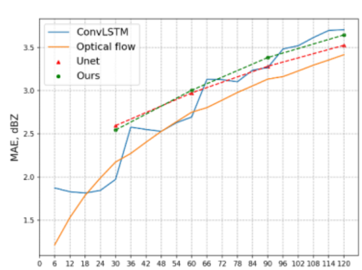

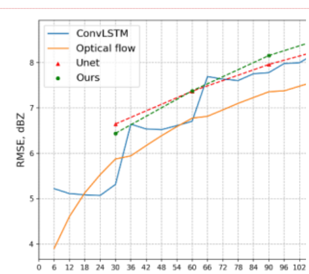

60 min **120 min**

~~(b)~~**30 min**

~~(a)~~

Optical Flow	0.316	0.391	0.439	0.474
ConvLSTM	0.265	0.295	**0.242**	**0.246**
U-Net	0.293	0.309	0.313	0.309
MSDM_mse	0.329	0.364	0.387	0.399
MSDM_ssim	**0.237**	**0.27**	0.303	0.335

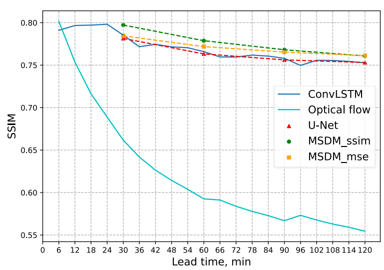

(a)

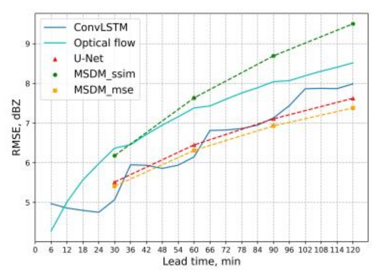

(b)

Figure 6. (a) ~~MAE~~SSIM of ~~four~~the five models~~, dBZ~~. (b) RMSE of ~~four~~the five models, dBZ.

We calculate the ~~mean absolute error (MAE) and root mean squared error (~~SSIM and RMSE~~)~~ between the predicted radar echoes of the four models and the ground truth on the ~~testing~~test set~~, respectively (Figure~~ (Fig 6). ~~the Optical~~The optical flow model ~~performs better than other models, while the U-net and MSDM model performs badly. We believe~~ achieves the lowest SSIM (Fig 6a), which means that it has the worst SSIM to the ground truth. MSDM_ssim obtains the highest score on the SSIM but the worst performance on the RMSE because it focuses on only local features but ignores the minimization of the global error. ConvLSTM, U-Net, and MSDM_mse are trained on the MSE loss function, which achieve a lower RMSE. We believe that when the SSIM is used as the loss function, the ~~CNN would focus on the local features and~~model will generate more reasonable predictions with proper shapes, but it will lead to ~~the bad~~poor performance ~~of the~~on global evaluation ~~index like~~ metrics such as the mean absolute error (MAE) and RMSE. ~~Meanwhile~~Moreover, we notice that the ConvLSTM model produces ~~bigger~~larger errors in the first frame of each sequence than other models. This phenomenon can result from the deficiency of LSTM that cannot handle accumulative error, which is magnified by ~~the way of~~ iterative prediction.

3.2~~.~~ QPN

Previous works seem to pay little attention to QPN after they ~~get~~achieve good performance on REE tasks. Researchers tend to use an empirical formula to calculate the precipitation rate based on the prediction of radar echo from models. Shi et al~~.~~. ~~(Shi et al., n.d.)~~(2015) employed the Z-R relationship ($Z = 10\,log\,a + 10b\,log\,R$) to calculate the rainfall, ~~here~~where Z represents the radar echo in the dBZ ~~and~~, R represents the rainfall rate in mm/h, and a and b are two constants that are calculated based on the statistical data of specific regions. We believe that this empirical formulation cannot describe the ~~non-linear~~nonlinear relationship between the radar echo intensity and the rainfall rate. Therefore, ~~the~~ random forest machine learning regression techniques ~~from machine learning~~ are used to describe this relationship. The weather radar data and precipitation data one hour before the prediction time are used for training. The method we take is as follows. ~~Firstly, looking for~~First, an automatic station~~.~~ is identified. Then, the radar and satellite data ~~on~~for these grid points as well as the corresponding rainfall rate from site points are applied to train the random forest model. Finally, the learned ~~non-linear~~nonlinear relationship is used to predict the rainfall rate an hour later.

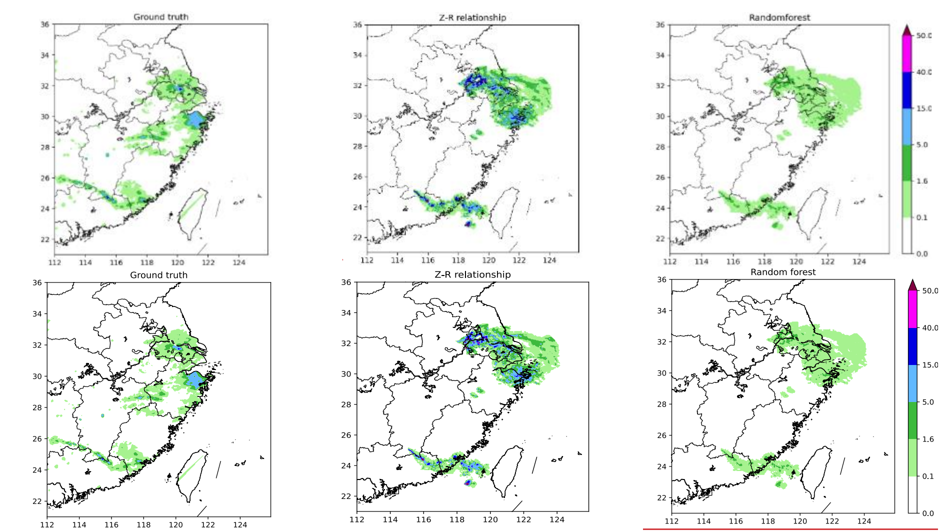

(**a**) (**b**) (**c**)

Figure 7. (a) Ground truth interpolated from site points, mm/h. (b) Rainfall rate calculated by the Z-R relationship, mm/h. (c) Rainfall rate calculated by the random forest model, mm/h

Formatted Table

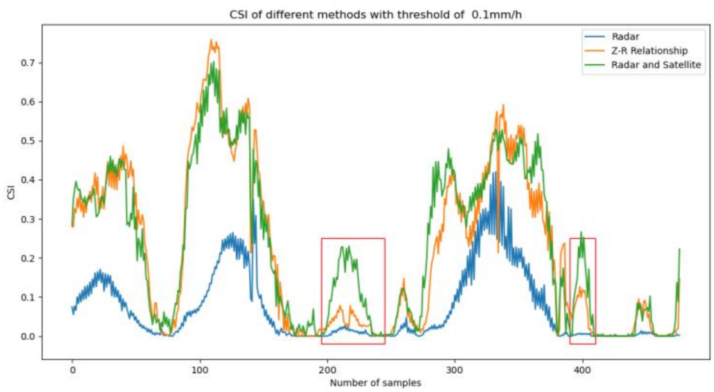
CSI of different methods with threshold of 0.1mm/h
Radar
Z-R Relationship
Radar and Satellite
CSI
Number of samples
0
100
200
300
400
0.0
0.1
0.2
0.3
0.4
0.5
0.6
0.7

~~(a)~~

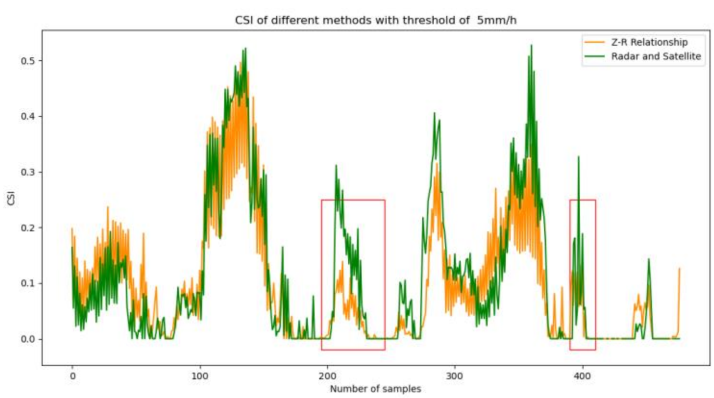
CSI of different methods with threshold of 5mm/h
Z-R Relationship
Radar and Satellite
CSI
Number of samples
0
100
200
300
400
0.0
0.1
0.2
0.3
0.4
0.5

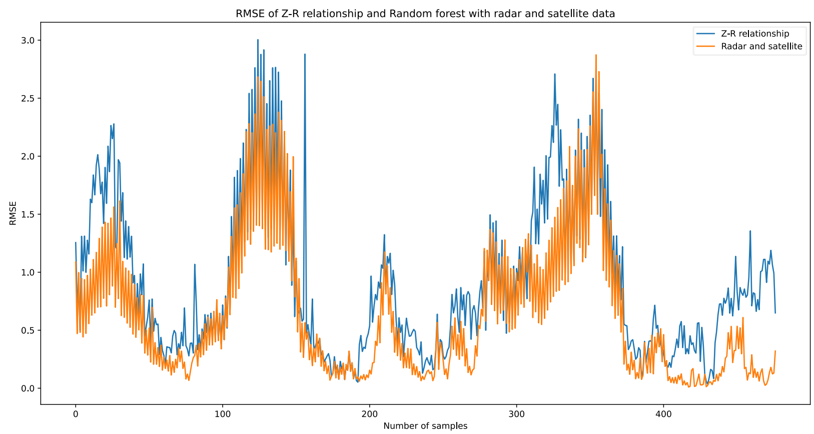

~~(b)~~

Formatted: Normal

Figure 8. ~~CSI~~RMSE of ~~selected~~ 480 QPN samples predicted by the two methods ~~with the threshold of 0.1mm/h (a), 5mm/h(b)~~

Figure 7 shows the results of the Z-R relationship and ~~Random~~random forest model. Since the precipitation data ~~onto~~on the grid points are obtained by ~~the~~ interpolation and might have errors, ~~so the~~we did not make a quantitative comparison ~~did not make.~~for the whole dataset. However, this example ~~could show~~shows that the Z-R relationship tends to overestimate the rain intensity. ~~Figure 8 shows CSI~~For example, the Z-R relationship predicts many areas with precipitation rates larger than 15 mm/h, but there are few areas that reach the value on the ground truth. Figure 8 shows the RMSEs of 480 QPN samples using different methods and data. When ~~only using~~we use the radar ~~data as the input its performance is poor. Because there is no precipitation in most of the areas, the Random forest may overfit~~ and ~~predict less rain. However, when we add the~~ satellite data as input, the ~~Random~~random forest ~~presents~~model shows its superiority in the QPN task. ~~Especially for~~Its RMSEs are lower than those of the Z-R relationship in most of the samples ~~in the red frames in Fig 8. Hence~~. Therefore, we believe ~~multi-source~~that multisource data ~~can~~have great potential to make the results more precise.

4. Conclusions and ~~discussions~~discussion

Discussion

In ~~order to predict QPN by machine learning based on the observed precipitation, the radar echo data, and Himawari 8 satellite brightness temperature data, we designed an image-to-image MSDM that uses the weather radar data and satellite data~~Table 4, we evaluate four models in terms of 12 performance indictors (amount of data required for training, time needed for training the model, false alarm rate, cumulative system error, ability to capture spatial/temporal characteristics, ability to predict the radar echo ~~30 minutes later. It performs well in the first hours with the threshold of 0.~~initiation and decay, 0~1 ~~dBZ and ranks second with a threshold of 40dBZ within 2 hours. The MSDM combines the merits from the Optical flow method and CNN~~hour forecast accuracy, 1~2 hour forecast accuracy, ability to maintain the radar echo shape, clarity of the radar image, conforming to the laws of physics). We use the mark '↓' to represent that the lower the better and the mark '↑' to represent the higher the better. Subsequently, we discuss and summarize the advantages and limitations of the models and their combinations.

Table 4. Evaluation on four models with the performance indictors

	Amount of data required for training ↓	Time needed for training the model ↓	False alarm rate ↓	Cumulative system error ↓
Optical flow	1	1	2	1
ConvLSTM	4	4	3	2
U-Net	2	2	4	2
MSDM	3	3	1	4

	Ability to capture spatial characteristics ↑	Ability to capture temporal characteristics ↑	Ability to predict radar echo initiation and decay ↑	0~1 hour forecast accuracy ↑
Optical flow	1	3	1	3
ConvLSTM	2	4	2	1
U-Net	3	1	3	2
MSDM	4	1	4	4

	1~2 hour forecast accuracy ↑	Ability to maintain the radar echo shape ↑	Clarity of the radar image ↑	Conforming to the laws of physics ↑
Optical flow	1	4	4	4
ConvLSTM	4	1	1	1
U-Net	3	2	2	2
MSDM	2	3	3	3

Here, the smaller the first four indictors values are (amount of data required for training, time needed for training the model, false alarm rate, cumulative system error), the better the model performance is; the larger the last eight indictors values are (ability to capture spatial/temporal characteristics, ability to predict the radar echo initiation and decay, 0~1 hour forecast accuracy, 1~2 hour forecast accuracy, ability to maintain the radar echo shape, clarity of the radar image, conforming to the laws of physics), the better the model performance is. Form Table 4 we can see that all of them have advantages and disadvantages. We are going to discuss the strong points and weak points of the methods.

Optical Flow:

The advantages of the optical flow algorithm are as follows: (1) It has the fewest parameters and takes the least time to train. (2) The amount of data required for training the model is small, and at least 2 radar images can be used to extrapolate the radar echo. (3) It maintains the shape of the radar echo very well, and the prediction result is closest to the real echo. Therefore, its MSE is the smallest. (4) It is suitable for the extrapolation of advection precipitation from 0 to 1 hour in the future.

The disadvantages of the optical flow algorithm are as follows: (1) It cannot extract features of the evolution process of the radar echo. (2) Except the advective precipitation, it performs poorly in other precipitation situations (e.g. convective precipitation and typhoon precipitation), in which the radar reflectivity changes rapidly in a short period of time. For the large-value area of radar echo, it basically has no forecasting ability. (3) The tail of the echo cannot be extrapolated due to the lack of previous data. As a result, the longer the lead time, the more irregular the shape of the echo at the tail.

ConvLSTM:

The advantages of ConvLSTM are as follows: (1) It can extract the spatial characteristics of echoes while capturing the time characteristics efficiently. (2) It can simulate the initiation and decay of radar echo better than optical flow. (3). It is the best for the prediction of long time and large-value areas of radar echo.

The disadvantages of ConvLSTM are as follows: (1) There are many parameters, many matrix operation and various gating structures in ConvLSTM. Therefore, its training speed is the slowest among the four models. (2) It overestimated/underestimated the large/lowvalue radar echo, which does not conform to the fluid continuity theory. (3) It predicts the worst shape of the echo in that there is no transition between the large echo area and the nonecho area, which is far away from the true echo and has no guidance for operational forecasting. For example, we cannot issue an early warning of heavy precipitation in one place, and at the same time it cannot forecast if there will be no rain in its neighboring places.

U-Net:

The advantages of U-Net are as follows: (1) It is an efficient CNN that has relatively few parameters and can achieve high accuracy with a small amount of data. (2) It is capable in capturing the spatial characteristics of radar echoes and predicting the evolution of echoes. (3) The forecasting effect is very good for the next one or two frames.

The disadvantages of U-Net are as follows: (1) It is unable to extract the temporal characteristics of changes in the radar echo. (2) The convolution operation will smooth the characteristics of the radar echo so that the shape of the predicted echo will change and deviate from the true one. (3) Through iterative training and prediction, the error accumulates.

Conclusions

As a conventional QPN method, the optical flow method has played a certain role in the forecasting of advective precipitation. However, it performs poorly in the prediction of advective precipitation due to the simplicity of its algorithm and the lack of use of existing big data (Woo and Wong, 2017). Moreover, deep learning shows great advantages in processing vast amounts of data. By using convolution and LSTM structures, deep learning algorithms are better at capturing spatiotemporal correlations. Nevertheless, recurrent networks (represented by ConvLSTM) for predicting spatiotemporal sequences are widely known to be difficult to train and computationally expensive (Yu et al., 2018). Compared with traditional spatiotemporal sequence tasks in the field of machine learning, such as moving Modified National Institute of Standards and Technology (MNIST) prediction, human position prediction, and traffic flow prediction, the REE task has specific background and physical constraints. Therefore, merely obtaining predictions with higher scores does not reflect the quality of the results. Wang et al. (2018,2019) designed state-of-the-art models to capture comprehensive correlations between spatiotemporal sequences. However, when we apply them to the physics-based tasks represented by REE and QPN, we must evaluate their prediction from the perspective of atmospheric science. The prediction is of reference significance only when it is physically reasonable rather than having high scores. However, it is difficult to apply physical constraints to neural networks due to their high degrees of freedom and nonlinearity. Hence, we input more kinds of data as features into the network with the intention that it can obtain more information through feature interaction. Therefore, we collect multisource data and design an MSDM. In a situation in which when the model becomes incorrect and tries to predict low radar reflectivity, the incorporated satellite data will balance it. We hope the multisource data function as another form of model constraint. Solving the sequence-to-sequence problem is computationally expensive, so we treat the QPN as an image-to-image problem and design the MSDM based on a CNN (U-Net) with high efficiency and few parameters. The main advantage of the MSDM is its transferability. Apart from satellite data, any other data (wind speed, pressure, temperature, etc.) can be used as input into the model in the future. Wind speed data could add dynamic constraints, and temperature data could add thermodynamic constraints. To further save computational resources, we use optical flow to predict the sequence of satellite data with the assumption that the cloud cluster is dominated by convective movement. This approach is adopted by an operational nowcasting system to estimate convective cloud movement (Shi et al., 2017). Subsequently, we use the satellite data predicted by optical flow and radar reflectivity predicted by the MSDM as input for iterative prediction to achieve a lead time of 2 hours. After predicting the radar echo, we replace the empirical formula (Z-R relationships) with a random forest model to estimate the rainfall rate. We believe that deep learning models capture the long-term trend in precipitation. There should be an algorithm that captures real-time dynamic characteristics, and random forest regression is very suitable for short-term prediction with small samples. Therefore, we trained a random forest regressor using radar and precipitation data from one hour prior. Subsequently, the learned nonlinear relationships were applied to estimate the precipitation rate from radar reflectivity.

In conclusion, the MSDM combines the merits of optical flow and U-Net, maintains the pattern of the radar echo, and predicts their initiation and decay. The results predicted by the MSDM also ~~contains~~contain more details that U-~~net~~Net cannot produce. ~~The~~Given the background that ConvLSTM~~ gets high scores for the strong radar echo, but it~~ overestimates the strong echo and underestimates the weak echo~~. In conclusion, it~~, the MSDM shows great potential in predicting areas of both strong and weak radar echo. We ~~make~~conducted an experiment by using ~~the~~ random forest for QPN, which ~~gets~~obtained relatively better results than ~~that~~those obtained by the Z-R relationship. ~~It proves~~This finding suggests that the empirical formula is not suitable for all areas. ~~So we~~We believe that by the combination of ~~multi-source~~multisource data, the radar echoes predicted by the MSDM ~~could~~can provide more details and have ~~fewer errors~~more physical constraints than those predicted by ~~the~~ single~~ observing data~~ observation data. It not only learns the long-term trend through deep learning but also incorporates real-time dynamic characteristics captured by the optical flow and random forest models. Hence, the prediction from the MSDM is more physically reasonable and of reference significance.

~~In this paper, we did not make any quality control for these data through training. Thus, the trained MSDM is more robust in the real case where there are missing data or noises. For REE task, we combined the Optical flow with Deep learning, in the future, there should be more work on the combination of multi-source data and RNNs. As for QPN, we make a trial on Random forest~~ Currently, methods still exist to estimate the precipitation~~. In this field, CNN should be considered for this task.~~ ~~Now there still exist methods to estimate precipitation~~ rate more precisely. For example, Wu et al~~(Wu et al., 2020). use Graph Convolutional Regression Network~~ (2020) used a graph convolutional regression network to produce more spatial characteristics of precipitation. For future works, we believe that the predictions could be more accurate with RNNs and GRUs. ~~Also~~Additionally, the precipitation rate should consider the influence of the terrain and different scales. In fact, we ~~are going to make~~will perform further experiments on these factors.

Code and data availability. ~~Rainymotion v1 is available at github repository https://github.com/hydrogo/rainymotion.~~ The source code and pretrained model of MSDM are ~~provided through google drive https://drive.google.com/drive/folders/1oEU_m0mZ2BssMeNTCDjkOBrFJg92LWOb?usp=sharing.~~ available at http://doi.org/10.5281/zenodo.4749183.

Formatted: English (United Kingdom)

Formatted: English (United Kingdom)

Formatted: English (United Kingdom)

Author contribution. Conceptualization, D.L., Y.L. and C.C.; methodology, software, investigation, D.L.; resources, data curation, C.C.; writing—original draft preparation, D.L.; writing—review and editing, Y.L.; visualization, C.C.; supervision, Y.L.; project administration, C.C.; funding acquisition, Y.L. All authors have read and agreed to the published version of the manuscript.

Competing interests. The authors declare that they have no conflict of interest.

Acknowledgements. This research is supported by the National Natural Science Foundation of China (41875060)

References

~~Aman, A. A. and Bman, B. B.: The test article, J. Sci. Res., 12, 135–147, doi:10.1234/56789, 2015.~~

~~Aman, A. A., Cman, C., and Bman, B. B.: More test articles, J. Adv. Res., 35, 13–28, doi:10.2345/67890, 2014.~~

Agrawal, S., Barrington, L., Bromberg, C., Burge, J., Gazen, C. and Hickey, J.: Machine Learning for Precipitation Nowcasting from Radar Images, arXiv:1912.12132 [cs, stat] [online] Available from: http://arxiv.org/abs/1912.12132 (Accessed 27 June 2020), 2019.

Ayzel, G., Heistermann, M. and Winterrath, T.: Optical flow models as an open benchmark for radar-based precipitation nowcasting (rainymotion v0.1), Geosci. Model Dev., 12(4), 1387–1402, doi:10.5194/gmd-12-1387-2019, 2019.

Ho, J., Kalchbrenner, N., Weissenborn, D., and Salimans, T.: Axial Attention in Multidimensional Transformers, 2019.

Ronneberger, O., Fischer, P., and Brox, T.: U-Net: Convolutional Networks for Biomedical Image Segmentation, in: Medical Image Computing and Computer-Assisted Intervention – MICCAI 2015, vol. 9351, edited by: Navab, N., Hornegger, J., Wells, W. M., and Frangi, A. F., Springer International Publishing, Cham, 234–241, https://doi.org/10.1007/978-3-319-24574-4_28, 2015.

Shi, X., Chen, Z., Wang, H., Yeung, D.-Y., Wong, W. and Woo, W.: Convolutional LSTM Network: A Machine Learning Approach for Precipitation Nowcasting, ~~,~~ 9, ~~n.d~~2015.

Shi, X., Gao, Z., Lausen, L., Wang, H., Yeung, D.-Y., Wong, W. and Woo, W.: Deep Learning for Precipitation Nowcasting: A Benchmark and A New Model, ~~,~~11, ~~n.d~~2016.

Sønderby, C. K., Espeholt, L., Heek, J., Dehghani, M., Oliver, A., Salimans, T., Agrawal, S., Hickey, J. and Kalchbrenner, N.: MetNet: A Neural Weather Model for Precipitation Forecasting~~,~~ , 17, ~~n.d~~2020.

Tran, Q.-K. and Song, S.: Computer Vision in Precipitation Nowcasting: Applying Image Quality Assessment Metrics for Training Deep Neural Networks, Atmosphere, 10(5), 244, doi:10.3390/atmos10050244, ~~2019a~~2019.

~~Tran, Q.-K. and Song, S.: Computer Vision in Precipitation Nowcasting: Applying Image Quality Assessment Metrics for Training Deep Neural Networks, Atmosphere, 10(5), 244, doi:10.3390/atmos10050244, 2019b.~~

Wang, Y., Gao, Z., Long, M., Wang, J. and Yu, P. S.: PredRNN++: Towards A Resolution of the Deep-in-Time Dilemma in Spatiotemporal Predictive Learning, arXiv:1804.06300 [cs, stat] [online] Available from: http://arxiv.org/abs/1804.06300 (Accessed 27 June 2020), 2018.

Formatted: Font: Bold, Font color: Black, English (United Kingdom), Kern at 16 pt

Formatted: Normal, Level 1, Space Before: 24 pt, After: 12 pt, Keep with next

Formatted: English (United Kingdom)

Formatted: English (United Kingdom)

Formatted: Normal, Space After: 12 pt

Formatted: Normal, Space After: 12 pt

Formatted: Normal, Space After: 12 pt

Wang, Y., Jiang, L., Yang, M.-H., Li, L.-J., Long, M. and Fei-Fei, L.: EIDETIC 3D LSTM: A MODEL FOR VIDEO PREDICTION AND BEYOND, ~~,~~ 14, 2019a.

Wang, Y., Zhang, J., Zhu, H., Long, M., Wang, J. and Yu, P. S.: Memory In Memory: A Predictive Neural Network for Learning Higher-Order Non-Stationarity from Spatiotemporal Dynamics, arXiv:1811.07490 [cs, stat] [online] Available from: http://arxiv.org/abs/1811.07490 (Accessed 29 June 2020b), 2019.

Wang, Z., Bovik, A. C., Sheikh, H. R. and Simoncelli, E. P.: Image Quality Assessment: From Error Visibility to Structural Similarity, IEEE Trans. on Image Process., 13(4), 600–612, doi:10.1109/TIP.2003.819861, 2004.

Woo, W. and Wong, W.: Operational Application of Optical Flow Techniques to Radar-Based Rainfall Nowcasting, Atmosphere, 8, 48, https://doi.org/10.3390/atmos8030048, 2017.

Wu, Y., Tang, Y., Yang, X., Zhang, W. and Zhang, G.: Graph Convolutional Regression Networks for Quantitative Precipitation Estimation, IEEE Geosci. Remote Sensing Lett., 1–5, doi:10.1109/LGRS.2020.2994087, 2020.

Yu, B., Yin, H., Zhu, Z.:Spatio-Temporal Graph Convolutional Networks: A Deep Learning Framework for Traffic Forecasting, 2018.

Formatted: Normal, Space After: 12 pt